BNL-67010-00/05-Rev.

COMPARISON OF MODEL ESTIMATED AND MEASURED DIFFUSE DOWNWARD SURFACE IRRADIANCE IN CLOUD-FREE SKIES

R. N. Halthore and S. E. Schwartz
Atmospheric Sciences Division
Environmental Sciences Department
Brookhaven National Laboratory
Upton, NY 11973-5000

Original Manuscript: December 1999
Revised: May 2000

Accepted for publication in
Journal of Geophysical Research
(in press)

By acceptance of this article, the publisher and/or recipient acknowledges the U.S. Government's right to retain a nonexclusive, royalty-free license in and to any copyright covering this paper.

Research by BNL investigators was performed under the auspices of the U.S. Department of Energy under Contract No. DE-AC02-98CH10886.

Comparison of model-estimated and measured diffuse downward irradiance at surface in cloud-free skies

Rangasayi N. Halthore and Stephen E. Schwartz

Environmental Sciences Department, Brookhaven National Laboratory, Upton, New York

Abstract. Diffuse downward shortwave irradiance at the surface arises from the scattering of radiation by molecules and aerosol particles. Recently, we reported that pyranometer-measured diffuse solar irradiance in cloud-free atmospheres is overestimated by radiative transfer models at two low-altitude sites by an amount that exceeds modeling and measurement uncertainties but is correctly estimated within these uncertainties at two high-altitude sites [*Halthore et al.*, 1998]. Here we explore this phenomenon in detail, with more cases and improved uncertainty analysis, confirming that the excess in modeled diffuse irradiance cannot be explained by uncertainties in measurements or aerosol-scattering properties that are input into the radiative transfer models or by errors in multiple-scattering schemes. The phenomenon is observed for all comparisons with data obtained intermittently over a 5-year period at the low-altitude sites. Model computations also exceed radiometer-measured sky radiance along the solar almucantar. Despite the inconsistencies between measured and modeled diffuse irradiance, atmospheric transmittance models correctly compute direct normal solar irradiance at all sites. These results indicate that at low altitudes a continuum atmospheric absorption process accounting for 0.022 ± 0.01 in vertical optical thickness at 550 nm, corresponding to 4 ± 2% absorptance, may need to be included in radiative transfer models and in models that retrieve aerosol optical thickness from extinction measurements. This is a substantial excess absorption with major implications for climate modeling and weather forecasting. In remote sensing studies, neglect of this excess absorption would lead to substantial errors in satellite sensor calibration and satellite inferred top-of-atmosphere flux. An agent or process for this absorption has not yet been identified.

1. Introduction

Direct-normal solar irradiance (E_{dir}), diffuse-downward irradiance (E_{dir}), and diffuse-upward irradiance at the surface ($E_{\mathrm{sfc}}^{\uparrow}$) represent, in order of increasing complexity, atmospheric radiation components that can be used to compare model calculations and measurements. Such comparisons test many aspects of atmospheric radiative transfer, including accurate measurement of relevant atmospheric properties and components of surface irradiance, precise knowledge and representation of atmospheric scattering properties in radiative transfer models, accurate computation of multiple-scattering processes in the same models, and accurate representation of solar spectral irradiance. These three irradiance components, which can be measured more easily at the surface than at altitude, provide an excellent set of parameters for evaluation of radiative transfer algorithms in climate models [*Halthore*, 1999]. Of these components, E_{dir} is the least complicated because it depends mainly on the atmospheric extinction, is not sensitive to surface reflectance, and furthermore, can be measured quite accurately (0.3%) by active cavity radiometry. For measurements at a midcontinental site, comparisons showed [*Halthore et al.*, 1997a, hereinafter referred to as paper 1] that model calculations were close to instantaneous measurements (fractional deviation, 0.2% ± 0.9%). This result thus established that (1) Sun photometer-measured atmospheric transmittance in narrow spectral bands throughout the visible and near-IR is accurate; (2) the model correctly interpolates and extends atmospheric transmittance between and beyond the Sun photometer channels in the shortwave (solar spectrum, 0.3-5 μm); (3) solar spectral radiance used in the model is accurate; and (4) E_{dir} measurement is accu-

rate. Comparisons of measured and modeled E_{dif} on the other hand show that for measured or inferred aerosol extinction, realistic aerosol-scattering properties, and for known bias errors in instantaneous E_{dif} measurements, model estimates consistently exceed measurements [*Kato et al.*, 1997; *Halthore et al.*, 1998, hereinafter referred to as paper 2].

The measurements of E_{dif} that comprise the basis of the present study were made with pyranometers. Other studies using different models and measurement schemes also indicate model overestimation of E_{dif}. Using pyranometer data and independently developed radiative transfer models, *Trishchenko and Li* [1998] and *Fu et al.* (1998) reported model overestimation of E_{dif} similar to that reported in paper 1. *Kato et al.* [1997] and *Harrison et al.* [1999], using silicon-based detectors, show that models overestimate (E_{dif} / E_{dir}) throughout the shortwave. *Richiazzi et al.* [1999] find model overestimation in diffuse radiance as obtained by an all-sky camera. *Charlock and Alberta* [1996] addressed the problem with closure in E_{dif} in comparisons of model estimates of components of irradiance at various altitudes, including the surface.

Why do model calculations exceed measurements of E_{dif}? Model calculations employ aerosol optical thickness (AOT) inferred from Sun photometric measurements of total extinction after subtracting known contributions from Rayleigh scattering and molecular absorption. Because of a consistent overestimate of E_{dif} it was concluded [*Kato et al.*, 1997; paper 2] that AOT inferred from Sun photometric measurements may have been overestimated by wrongly attributing an unknown atmospheric continuum-like absorption to aerosol extinction; it should be noted that comparison of measured and modeled E_{dir} does not distinguish between absorption and scattering.

In this paper, we examine the measurement errors and model uncertainties in greater detail than could be presented previously. We analyze data from two low-altitude and two high-altitude sites. The low-altitude sites are mid-continental sites, in the boreal forest of Saskatchewan, Canada (BOR, 53.92˚ N, 104.69˚ W, 510.5 m altitude; 53.90˚ N, 106.1˚ W, 550 m altitude) and the Atmospheric Radiation Measurement (ARM) program Southern Great Plains (SGP) site in North-Central Oklahoma (36.605˚ N, 97.485˚ W, 319 m altitude). The two high-altitude sites are the summit of Mauna Loa in Hawaii (MLO, 19.533˚ N, 155.578˚ W, 3,400 m altitude) and the Amundsen-Scott observatory at the South Pole (SPO, 89.98˚ S, 24.8˚ W, 2,800 m altitude).

The impetus for this work arises in part from earlier reports of excess absorption in cloudy [*Stephens and Tsay*, 1990; *Cess et al.*, 1995; *Pilewskie and Valero*, 1995; *Ramanathan et al.*, 1995; *Li et al.*, 1995; *Charlock and Alberta*, 1996; *Imre et al.*, 1996] and cloud-free atmospheres [*Wild et al.*, 1995; *Arking*, 1996; *Charlock and Alberta*, 1996]. Here the term “excess absorption” refers to a portion of total absorption that is due to an unknown absorber or process and is not currently represented in atmospheric radiative transfer and transmission models. Some of these studies indicated that the magnitude of this excess absorption in cloud-free and/or cloudy skies is sufficiently large to significantly impact current understanding of radiative transfer processes in the atmosphere and hence climate [*Wiscombe*, 1995; *Kiehl and Trenberth*, 1997]. Atmospheric absorption is a key process that accounts for about 20% of the solar radiation and about 20% of the longwave emission to space (which is 70% of incoming solar energy). Several of the previous studies used measured, inferred, or estimated values of irradiance components at altitudes and at the surface to deter-

mine atmospheric absorption. Our calculations (paper 2) indicate that atmospheric absorption in cloud-free atmospheres could be as great as 25% of the incoming solar energy in the shortwave. An important feature of the current study (and that of *Kato et al.* [1997]), unlike many of the earlier works, is that the comparisons are made with instantaneous measurements; that is, no temporal averaging is performed. The model inputs correspond to instantaneous values that are obtained simultaneously or nearly simultaneously with the irradiance measurement. An additional advantage of this approach is that no satellite data are used in this study, eliminating uncertainty associated with satellite sensor calibration, wavelength response, and radiance to flux conversion.

Below, we discuss first irradiance measurement issues followed by uncertainties in model inputs, in particular, aerosol-scattering properties and surface reflectance. In section 3 we discuss the magnitude of the excess absorption relative to measurement and model uncertainties, consider additional evidence, and briefly discuss implications of the excess absorption for climate modeling and remote sensing.

2. Measurements and Models

2.1. Irradiance Measurement With Pyranometers

The diffuse downward irradiance measurements reported here are obtained with pyranometers that are ventilated and shaded (precision shaded pyranometers, Eppley Laboratory, Inc., Newport, Rhode Island). The sensing element in a pyranometer is a flat thermopile detector that has been blackened to absorb the shortwave radiation when exposed to the hemispherical sky. Two hemispherical fused silica glass domes above the sensing element provide wavelength selectivity (0.29 to 2.9 μm) and keep the detector free of precipitation, dew, and dust. Ventilation by forced airflow over the outer dome provides control over convective and conductive heat losses and prevents condensation. In the unshaded mode the pyranometer measures total or global surface irradiance; in the shaded mode (where a shadow band or a shadow disk obstructs the Sun's disk) it measures diffuse surface irradiance. Anisotropy in the sensor response to hemispherical downward irradiance is a major source of uncertainty, preferentially affecting measurements in the unshaded mode, in which the direct beam contributes the bulk of the irradiance. An ideal detector would exhibit a perfect cosine response for illumination at different zenith angles and would not exhibit sensitivity to azimuth angle. In reality, all surfaces have imperfections resulting in deviations from an ideal cosine response and, furthermore, reflect an increasing fraction of incident radiation at large zenith angles. Thus the actual response must be characterized fully, and calibration must account for this lack of ideal cosine response.

2.1.1. Calibration. The basis of absolute calibration of pyranometers is the use of the electrical substitution devices such as active or absolute cavity radiometers (ACRs) which measure the direct solar irradiance in a narrow field of view (~5˚) to an accuracy of about 0.3%. In the so-called sunshade technique a pyranometer is alternatively shaded and unshaded to obtain diffuse and total, or global, components of irradiance, respectively; the difference between them is the downward component of the direct-normal irradiance, which is then compared with that measured by the ACR. This technique has been used to calibrate pyranometers at SGP (T. Stoffel, National Renewable Energy Laboratory, Golden, Colorado, private communication, 1997) and

Baseline Radiation Network (BSRN) Sites at SGP, MLO, and SPO [*Forgan*, 1996]. An alternative method can also be used whereby the response of a pyranometer to be calibrated is compared to a reference or primary pyranometer, which has itself been calibrated by the sunshade technique in comparison with the response of a group of ACRs comprising a core group of standard irradiance measurement devices at Davos, Switzerland [*Forgan*, 1996].

A critical shortcoming of the sunshade technique is its inability to determine zero offset, i.e., the pyranometer response in the absence of shortwave irradiance (see below). Such a zero offset is manifested (Figure 1) as negative apparent irradiance values at night, when the shortwave irradiance is essentially zero. In Figure 1, pyrheliometer-measured E_{dir} and shaded pyranometer-measured E_{dif} are plotted as a function of time for a cloud-free day. The instruments belong to two groups of instrumentation at SGP with independent calibration protocols (BSRN), a worldwide network maintained at SGP by NOAA, and solar and infrared radiation system (SIRS), a local network maintained by ARM. Throughout the night, and even at and after sunrise identified by a rapid increase in E_{dir}, the apparent E_{dif} values obtained by both pyranometers are negative, contrary to observation that diffuse skylight precedes sunrise by about half an hour. Analysis at sunset shows that E_{dif} is likewise negative during dusk. Thus the mechanism responsible for the nighttime offset is apparently operative not just at night but also under conditions when shortwave irradiance is incident on the detector. This zero offset must be correctly accounted for in estimating E_{dif}. If the offset is not properly accounted for, especially at low apparent AOTs, measurements may indicate a so-called Rayleigh problem (R. D. Cess et al., Consistencies and inconsistencies in measured total, direct and diffuse shor4twave radiation at the surface, submitted to *J. Geophys. Res.*, 1999) wherein the uncorrected E_{dif} is less than the calculated E_{dif} for a Rayleigh (aerosol free) atmosphere. If, on the other hand, E_{dif} is overcorrected for the zero offset, measured values would be much higher than the maximum permitted for modeled values; such could be the case at a location such as MLO, where Sun photometer-inferred AOT is essentially zero. The zero offset is thought to arise from radiative and/or convective cooling of the sensing element. Below, we explore the reason for the existence of the offset and describe and evaluate a method [*Wardle and Barton*, 1988; *Wardle et al.*, 1996; E. Dutton, NOAA, Boulder, Colorado, private communication, 1998] for determining the daytime offsets using simultaneous pyrgeometer measurement of net longwave downward irradiance.

Figure 1

2.1.2. Origin of zero offset. For horizontal downward irradiance E, let the voltage response V of an ideal pyranometer with perfect cosine response be expressed as

$$V = R' E + V_0' \ , \qquad (1)$$

where R' is the calibration coefficient in volts/(W m^{-2}) and V_0' is the offset voltage composed of three components: (1) an electrical component unrelated to electromagnetic radiation or to heat balance, (2) a component due to all forms of instrument cooling that is shortwave independent, and (3) a component due to all forms of instrument cooling that is shortwave dependent. Thus assuming that the zero offset is a constant plus a term that is linearly dependent on irradiance to first order,

$$V_0' = V_0 + \alpha E \ , \qquad (2)$$

where V_0, the constant, represents the shortwave-independent portions (1) and (2), and αE represents the shortwave-dependent portion (3). In general, both terms on the right-hand side of equation (2) depend on factors that affect cooling, specifically, longwave cooling. Substituting for V_0' in (1) we obtain,

$$V = (R' + \alpha)\, E + V_0 = R\, E + V_0 \quad . \qquad (3)$$

Here $R = R' + \alpha$, from which it is seen that $E = (V\text{-}V_0)/R$. If V_{sh} and V_{us} are the voltages measured in the shaded and unshaded mode, respectively, then,

$$R = (V_{us} - V_s) / (E_{us} - E_s) = (V_{us} - V_s) / (E_{dir} \cos \theta), \qquad (4)$$

where θ is solar zenith angle. Direct irradiance E_{dir} is measured by an ACR. Thus determination of R by calibration includes the shortwave-dependent component of cooling to first order. For nonideal pyranometers, R must be determined at various solar zenith angles, and the procedure, performed for instruments used here, is quite tedious.

The zero offset V_0, about which no information is obtained by this calibration technique, is determined first by measuring the voltage for zero shortwave irradiance, i.e., at night. The value at night at SGP and MLO generally varies from night to night between –5 W m^{-2} and –10 W m^{-2}. In paper 2, daytime offsets were determined by linear interpolation between two cloud-free nights bracketing the day in question. A similar procedure was adopted for data obtained at BOR (R. Shewchuk, Saskatchewan Research Council, Saskatoon, Canada, private communication, 1997). At SPO a pyranometer calibrated in comparison with a reference pyranometer with zero nighttime offset was used.

Methods other than simple interpolation or extrapolation of nighttime offsets are sometimes recommended for estimating daytime offsets [*Wardle and Barton*, 1988; E. Dutton, NOAA, Boulder, Colorado, private communication, 1998]. In one method, net longwave downward irradiance as measured by an uplooking pyrgeometer is taken to be a surrogate for the longwave instrumental cooling to the atmosphere and is used to estimate the magnitude of the offset. The construction of the pyrgeometer is similar to that of a pyranometer except that the instrument is sensitive to the thermal IR region of the spectrum rather than the shortwave. Net longwave downward irradiance becomes more negative during the day (Figure 2a), indicating increased cooling to the atmosphere when the instrument and the substrate absorb shortwave radiation and, consequently, heat up. Use of the pyrgeometer signal as a surrogate is suggested by observed correlated variations in the net longwave irradiance and pyranometer offset signal at night under cloudless skies. In Figure 2b, nighttime pyranometer offset signal is plotted against pyrgeometer-measured net longwave downward irradiance for cloudless nights bracketing a day in December 1997 at MLO. The observed linear relationship between the two variables (r^2=0.4, where r is the correlation coefficient) is then applied to the observed daytime net longwave flux to infer the daytime offset. Estimates of the daytime offsets by this approach were performed for all the measurements at SGP and MLO on days for which the previous and/or successive nights had cloudless periods. Cloudless periods were ascertained by inspection of nighttime traces of both net longwave irradiance and pyranometer signal. Daytime offsets thus estimated agreed with those obtained by simple interpolation of nighttime offsets within ~1 to 2 W m^{-2} (Figure 3) with few exceptions. The exceptions, for which the difference was over 2 W m^{-2}, occurred in

Figure 2

Figure 3

the afternoon, when the net longwave radiation to the atmosphere was a maximum. This agreement between the two estimates is consistent with the finding of *Wardle and Barton* [1988]. Other surrogates to estimate daytime offsets such as the temperature difference between the sensor and the dome, have recently been proposed [*Bush et al.*, 1999].

Pyranometer response, and therefore, the offset, is found to be sensitively dependent on whether or not the instrument is ventilated [*Ohmura and Schroff*, 1983]; all the data discussed in this work are from pyranometers with ventilation. Figure 1 shows that two independent pyranometers would yield the same daytime measurements of E_{dif} using the procedure outlined in the previous paragraph (Figure 2), leading to the conclusion that the mechanism giving rise to the offsets is the same for both instruments and does not depend on differences in the details of the construction or characteristics of the components of these instruments.

2.1.3. Other corrections. Cavity radiometers are used without windows during calibration of other instruments and, consequently, are sensitive to radiation at all wavelengths of the solar spectrum. Pyranometers, on the other hand, typically use Schott glass (WG 295, Schott Glass Technologies, Duryea, Pennsylvania) or quartz windows that restrict their wavelength range to 0.28 to 2.9 μm. Thus a correction needs to be made for any changes in surface irradiance or, more specifically to a very good approximation, atmospheric transmittance, outside this wavelength range from the time of calibration. Such changes are due mainly to changes in water vapor abundance. Model runs to estimate the magnitude of this effect show that the required correction is typically less than 1 W m^{-2}. Here this effect is treated as contributing to an uncertainty rather than to a correction because water column abundance is not usually recorded at the time of calibration.

In pyranometers with disk shading (at all sites except BOR) the occulting disk covers about 5.7° around the Sun, thus blocking a significant portion of the aureole brightness. A calculation with MODTRAN 3.5 shows that a correction of approximately 1 W m^{-2} is needed to account for this. For pyranometers with a shadow band (BOR sites) the required correction was much larger, 8% of measured E_{dif} (~4 W m^{-2} at 50 W m^{-2}), because a larger area of the sky is blocked.

2.1.4. Uncertainty in E_{dif} measurement. The uncertainty in the measured E_{dif} is difficult to quantify because of unknown uncertainty in the magnitude of daytime offsets using the above procedure. We find that at high altitudes in essentially Rayleigh atmospheres pyranometers using same calibration protocols and procedures to estimate daytime zero offsets as those at low altitudes measure E_{dif} to within a few watts per square meter of model-estimated values. As discussed below, this lends support to the calibration procedure and to the method of estimating zero offsets. On the basis of experience in using a large number of pyranometers to measure E_{dif} under identical conditions, it is concluded (E. Dutton, NOAA, Boulder, private communication, 1998) that with the above correction procedure for the offsets, the expected uncertainty in measured E_{dif} is ±5 W m^{-2} at the 75% confidence level and ±8 W m^{-2} at the 95% confidence level.

2.2. Aerosol Optical Properties

Aerosol optical thickness inferred from Sun photometers is available at SGP, BOR, and MLO sites. Sun photometers (model CE318, Cimel Electronique, France) belonging to the NASA

Aerosol Robotic Network (AERONET) [*Holben et al.*, 1998] are used here to measure the atmospheric total vertical optical thickness to an accuracy of ±0.01 in eight discrete wavelength channels of 10 nm width centered at 340, 380, 440, 500, 670, 870, 940, and 1020 nm. In all channels, except the one at 940 nm coinciding with a water vapor absorption band, the apparent vertical aerosol optical thickness (AOT), defined as the total optical thickness minus optical thickness contribution from Rayleigh scattering and known gaseous absorption, all referred to vertical, was derived using extinction due to Rayleigh scattering and current knowledge of molecular band and continuum absorption. The nonwater vapor Sun photometer channels were chosen to avoid gaseous absorption bands other than Chappuis ozone bands, which are broadly distributed throughout the visible spectrum but whose absorption properties are thought to be well characterized. Ozone optical thickness was determined by multiplying climatological abundance with measured ozone absorption coefficient for each channel. When possible, climatological values of ozone column abundance were checked with satellite (TOVS) [*Neuendorfer*, 1996] measurements. Some water vapor absorption is present at 500 nm, with optical thickness in very humid atmospheres (vertical column abundance of water or precipitable water, PW = 4.3 cm) as great as 0.01, but no correction was made for this in the data analysis. The Ångström exponent (β in $\tau = a\,\lambda^{-\beta}$, where τ is the AOT and λ is the wavelength) was determined by fitting a least squares line through points in a plot of ln τ versus ln λ.

At SGP an integrating nephelometer (TSI, Minneapolis, Minnesota, model 3653) measures the aerosol-scattering coefficient σ_{sp} and hemispheric backscattering coefficient σ_{bsp} at wavelengths 450, 550, and 700 nm by sampling a dried stream of air (relative humidity, RH = 20% - 40%) from a 10-m-high stack. A particle soot absorption photometer (PSAP, Radiance Research, Seattle, Washington) measures the aerosol absorption coefficient, σ_{ap}, at a wavelength of 565 nm. These measurements have been made since July 1996, and when available, they enable calculation of single-scattering albedo ω_0, evaluated as $\sigma_{sp}(550)$ / [$\sigma_{sp}(550)+\sigma_{ap}(565)$]. The surface-measured values of ω_0 are likely to be underestimates for aerosols in the whole vertical column since the measurements are made in a dried stream, and furthermore, atmospheric RH usually increases with height during daytime. For cases for which ω_0 was not measured a value of 0.94 was used. The asymmetry parameter g was determined from the backscattering to total scattering ratio (σ_{bsp} /(σ_{sp}) as measured in the nephelometer [*Marshall et al.*, 1995]. The uncertainty in the estimates of ω_0 is expected to be no more than 6% [*Anderson et al.*, 1999]. For g the uncertainty is assumed to be 0.1 (J. Ogren, NOAA, Boulder, private communication, 1998). Because in situ measurements of aerosol optical properties were not available at other sites, values for these quantities were assumed for model simulations; for the cases considered here, aerosol loading was minimal at BOREAS and the high-altitude sites, and consequently, the calculations are insensitive to these parameters.

2.3. Atmospheric and Surface Properties

At SGP and BOR, radiosondes were launched frequently to measure temperature and relative humidity (RH) as a function of pressure. At MLO, such data are available only at 0000 UT and 1200 UT; for other times, Sun photometer-measured PW is used. Climatological values are used for the SPO site. PW measured by radiosondes agrees with that measured by Sun photometer (using

the 940-nm channel) and microwave radiometer to within ±10% [*Halthore et al.*, 1997b]. Ozone column abundance was described as above. In many cases, reported in paper 1, the discrepancy between models and ACR measurements of E_{dir} could be completely explained by the uncertainty in ozone column abundance.

Diffuse irradiance at the surface E_{dif} depends on the surface albedo because of multiple reflections between the surface and the atmosphere; the higher the surface albedo for a set of atmospheric conditions the higher the measured (and calculated) E_{dif}. For SGP, reflectance measurements made at a similar site in Kansas were used [*Walter-Shea et al.*, 1992]; for BOREAS, albedo inferred from surface fluxes was used [*Betts and Ball*, 1997]; for SPO a constant (visible and near IR) value of 0.82 for aged snow was used [*Warren and Wiscombe*, 1981]; for MLO a value of 0.05 (constant) pertaining to black lava was used.

2.4. Sky Radiance Measurements With Sun Photometers/Radiometers

Calibrated sky radiance measurements were made with Sun photometers/ radiometers under cloud-free skies at BOR. Sun photometers belonging to AERONET (previously described) were used in the radiometric mode. In this mode, sky radiance in W m^{-2} sr^{-1} μm^{-1} is directly measured with a large aperture collimator and increased detector gain in four channels: 440, 670, 870, and 1020 nm. Calibration was performed using an integrating sphere source itself calibrated in reference to standard lamps to an accuracy of ±5%. Sky scans along the solar almucantar (variable azimuth angle at constant zenith angle equal to the solar zenith angle) and along the solar principal plane (variable zenith angle at constant azimuth angle equal to the solar azimuth angle) provide radiance as a function of scattering angle.

2.5. Models

MODTRAN 3.5 (V1.5) [*Anderson et al.*, 1995; *Bernstein et al.*, 1996; *Berk et al.*, 1998] is a widely used moderate resolution (2 cm^{-1}) radiative transfer program is used with either of two models: a two-stream Isaacs model and a multistream discrete-ordinate model (DISORT) [*Stamnes et al.*, 1988]. In the Isaacs model in MODTRAN, corrections for spherical geometry include computing solar irradiance in each layer along a curved path to the Sun. The DISORT model, on the other hand, assumes a plane parallel atmosphere. The Second Simulation of Satellite Signal in the solar Spectrum (6S) model is a moderate resolution (10 cm^{-1}) specialized atmospheric correction model that uses Successive Order Approximation to solve the radiative transfer equation [*Vermote et al.*, 1997]. It performs radiative transfer in the wavelength range 0.25-4.0 μm, from which the results are extrapolated to the full wavelength range as described below. All three models use parameterized band models that are based on HITRAN database compiled at the Hanscom Air Force Base. This database is updated periodically [*Rothman*, 1998] and is considered to represent current knowledge of absorption by all known bands of gases and vapors in the atmosphere. A majority of the band strengths available in the database is model generated, but the most important bands are experimentally determined. In addition, both models include continuum absorption due to water vapor, ozone, and a number of other gases. Apparent AOT as determined by a Sun photometer is input as a function of wavelength, in

MODTRAN by directly specifying extinction coefficient, and in 6S by specifying aerosol size distribution to yield measured extinction. Both single-scattering albedo and asymmetry parameter are specified as constants with wavelength. In MODTRAN two phase functions were used: the Henyey-Greenstein phase function and a phase function based on Mie-scattering calculations. The flux (W m^{-2}) output of MODTRAN at each wavelength was integrated over a wavelength to yield total shortwave flux at the surface. The radiance output of 6S at several predetermined azimuth and zenith angles was integrated over an angle to yield fluxes. It is expected that the multistream DISORT calculations more correctly represent multiple-scattering, especially at large solar zenith angles (see Table 1 and associated discussion, below).

Table 1

2.6. Corrections to Model Estimates

Model calculations of E_{dif} are restricted to the spectral range 0.3 to 5 μm (MODTRAN) and 0.25 to 4 μm (6S). Solar energy in the direct beam at the surface beyond 5 μm is about 0.1% of the total (paper 1) and marginally higher for 6S; computed E_{dif} is increased by this amount. Use of a slightly higher solar constant (1372 W m^{-2} in MODTRAN and 6S), as opposed to the generally accepted value of 1366 W m^{-2}, requires that the calculated values of E_{dif} and E_{dir} be decreased by about 0.5% (paper 1).

3. Results and Discussion

Results for forty-three cases are summarized in Table 1. In this table, each comparison, designated by a case number in column 1, is characterized by a unique set of atmospheric properties and illumination geometry. Some cases (4 and 5, for instance) differ only in a limited way (solar zenith angle, column 4) and are included to illustrate the lack of dependence of the overestimate on the actual instant of comparison. Cases for the same day that differ from each other by more than 3 hours use different radiosonde profiles of temperature and humidity. Cases 17 to 23 illustrate the effect of the solar zenith angle. Cases 39 and 40 refer to the same time but two different locations within the BOR site, about 100 km apart. For the high-altitude cases 41 to 43 the model runs, with very little or no aerosol extinction, calculate E_{dif} values close to those measured. Comparisons were performed under conditions of varying solar zenith angle (27° to 82°), apparent AOT at 550 nm (τ_{550}, column 5, 0.03 to 0.24), Ångström exponent β (column 6, 0.5 to 1.6) and precipitable water PW (column 9, 0.11 to 4.6 cm). Measured values of E_{dif} range from a low of 26 W m^{-2} at MLO to 29 W m^{-2} at high zenith angle at SGP to a high of 141 W m^{-2} at SGP under relatively high turbidity conditions (τ_{550} = 0.24). Data were obtained between 1994 (BOR) and 1998 (SGP). All measured E_{dif} values at SGP and MLO (column 11) were corrected by using nighttime offsets scaled by net longwave flux to obtain daytime offsets (column 10), as described in the previous section. Measured values at BOR and SPO were acquired either with zero offsets applied or did not require offset correction as described section 2.

Results show that (Table 1) for the low-altitude sites SGP and BOR, model estimates of E_{dif} (columns 12 and 13) were consistently greater than measured values (column 11) by an average 18 W m^{-2} (column 14 = column 13 – column 11) or 19% of measured. Model evaluation using the two-stream method

(column 12) erroneously tends to show better agreement with measurements at large solar zenith angles (as also indicated by low $\Delta\tau_{550}$) because of underestimation of multiply scattered energy. The eight-stream DISORT simulation with more reliable multiple-scattering computation continues to show (column 13) the overestimate in E_{dif} for these long path lengths where multiple scattering is important. For the high-altitude cases the modeled values are quite close to measured (2 W m^{-2} or 5% of measured). We now examine the uncertainties associated with these comparisons.

3.1. Uncertainty in Modeled E_{dif}: Sensitivity to Input Parameters

The uncertainty in model computation of E_{dif}, δE_{dif}, is dependent to varying degrees on the uncertainty in input parameters AOT, ω_0, g, surface reflectance ρ, Ångström exponent β, and PW in addition to the input parameters themselves (i.e., the base conditions). The uncertainty in the computation of E_{dif} arises also from the type of radiative transfer model used. For low τ_{550} (<0.1), δE_{dif} is most sensitive to δAOT, the uncertainty in AOT (paper 2). For intermediate to high τ_{550} (0.1-0.3), $\delta\omega_0$, the uncertainty in single-scattering albedo has the greatest effect (see below). If the uncertainties in the above quantities are not correlated, δE_{dif} can be expressed as

$$\delta E_{dif} = \left[\sum_i \left(\frac{\partial E_{dif}}{\partial \chi_i} \right)^2 \delta\chi_i^2 \right]^{1/2} \qquad (5)$$

Here χ_i represents the ith model input parameter and $(\partial E_{dif} / \partial \chi_i)$ represents the sensitivity, defined as the change in the computed E_{dif} for a unit change in the ith input parameter, keeping all others constant.

The sensitivities of calculated E_{dif} to changes in ω_0, g, and ρ, respectively, for two cases, case 27 and case 37, representing low and high AOT are shown in Figure 4. The quantity plotted is the difference between modeled and measured E_{dif}, the latter being a constant for each curve. The slope $(\partial E_{dif} / \partial \chi_i)$ is computed for the two cases shown in these figures and, additionally for an intermediate AOT case (case number 34 in Table 1) and summarized in Table 2 (columns 3, 5, and 6). Also summarized in Table 2 is the sensitivity to change in AOT itself (column 4). The sensitivity of E_{dif} to PW and β (not shown in Table 2) is found to be negligible in comparison with the tabulated terms; a 10% uncertainty in PW leads to an uncertainty in E_{dif} of 0.5 W m^{-2}, negligible compared to the other sensitivities. Likewise, the calculated irradiance is relatively insensitive to the use of different models. For example, for the same inputs, calculations of two-stream MODTRAN and 6S compare to within 1 W m^{-2} for most cases, indicating that the computed E_{dif} is not sensitive to the specific multiple-scattering scheme employed. In some cases, larger differences of 4-7 W m^{-2} (Table 1) between eight-stream and two-stream MODTRAN models may indicate insufficient accounting for multiple scattering in two-stream models.

Comparison of the product of the sensitivity and the uncertainty for each component shows (Table 2) that for high AOT, uncertainty in E_{dif} is dominated by the uncertainty in ω_0 ($\delta\omega_0$ = 6%) followed by the uncertainty in g (δg = 0.1), and then by the contribution due to $\delta\tau$ (=0.01). For low and intermediate AOT, contribution to δE_{dif} due to the uncertainties in AOT and ω_0 are

Figure 4

Table 2

comparable. If a measurement of ω_0 is available, it is likely to represent the lower limit, as discussed in section 2. However, to be conservative in estimating the magnitude of the discrepancy between modeled and measured E_{dif}, we use symmetric error bars about the measured value of ω_0 to estimate uncertainty in the calculated E_{dif}. In all the simulations we have used ω_0 as a constant with wavelength. A more realistic case with Mie calculated ω_0, depicts significant absorption beyond 1 μm, yielded values within 0.2% of E_{dif} calculated assuming ω_0 as a constant.

The uncertainty in ΔE_{dif}, the difference between modeled and measured E_{dif}, is given by,

$$\delta\left(\Delta E_{\mathrm{dif}}\right)=\left[\left(\delta E_{\mathrm{dif}}^{\mathrm{modeled}}\right)^2+\left(\delta E_{\mathrm{dif}}^{\mathrm{measured}}\right)^2\right]^{1/2} \qquad (6)$$

where it is assumed that the measured and modeled uncertainties are uncorrelated. Substituting for the uncertainty in the measured value of 5 W m^{-2} (75% confidence level) and 8 W m^{-2} (95% confidence level), yields estimates of $\delta(\Delta E_{dif})$ given in column 8 of Table 2. Thus for case 27 (low AOT) the uncertainty in ΔE_{dif}, $\delta(\Delta E_{dif})$, is ±8.4 W m^{-2} at the 75% confidence level and ±10.5 W m^{-2} at the 95% confidence level. For case 34 (intermediate AOT) the corresponding uncertainties are ±10.7 W m^{-2} and ±12.4 W m^{-2}, and for case 37 (high AOT), the uncertainties are ±14.8 and ±16.0 W m^{-2}, respectively. Thus the uncertainty limits increase with increasing AOT. For most cases in Table 1, inferred τ_{550} is between 0.06 and 0.24; the uncertainty correspondingly falls within the above limits.

For all cases pertaining to low-altitude sites (Figure 5), ΔE_{dif} is positive; that is, the model overestimates the measured diffuse irradiance. In Figure 5 the cases are classified into three groups, low AOT ($\tau_{550} \leq 0.1$), intermediate AOT ($0.1<\tau_{550}<0.2$), and high AOT ($\tau_{550} > 0.2$), to enable drawing of the uncertainty bars as a function of AOT according to Table 2 (column 8). Twenty-six cases out of 40 indicate model overestimation at the 75% confidence level (22 out of 40 cases at 95% level). It is relevant to point out that if the estimates of daytime offsets are substantially greater, as for example implied in the work of *Bush et al.* [1999], then estimates of measured values would be close to modeled ones. However, there would then be a reverse problem at high altitudes (see below): the models would underestimate measurements.

In contrast to the results at low-altitude sites SGP and BOR, at high altitudes (cases 41-43), model-calculated E_{dif} agrees with measurements to well within the uncertainties due to model inputs and measurements. Because the measured τ_{550} at MLO was only 0.01, the main contributions to the uncertainty in modeled E_{dif} arise from the uncertainty in the surface reflectance and the AOT; it is estimated to be ± 5.8 W m^{-2}. At MLO, E_{dif} was corrected for offsets using simultaneously measured longwave irradiance, as described above. If the actual daytime offsets were substantially greater than the offsets obtained by this procedure, then the measured E_{dif} would correspondingly exceed the modeled values. As the extinction due to Rayleigh scattering is accurately estimated (using the surface pressure), the only way to increase the irradiance in the models would be to increase AOT. However, such an increase in AOT would upset the excellent closure in E_{dir} that is achieved at MLO. Thus it is unlikely that the daytime zero offsets are much greater than the scaled nighttime offsets. In

Figure 5

Figure 5, high-altitude cases have smaller uncertainty limits (±6 W m^{-2}) than the low-altitude cases because of the low AOT.

3.1.1. Almucantar sky scans. Radiance measured along the solar almucantar using the Cimel Sun photometer radiometer on a clear day at Boreal Ecosystem Atmospheric Study (BOREAS) is shown (Figure 6) as a function of scattering angle. It can be seen in the figure that model (MODTRAN) estimates of sky radiance obtained with two-stream and eight-stream multiple-scattering schemes using measured atmospheric properties as input are higher than observations at all scattering angles except angles very close to the Sun. Lack of adequate out-of-view light rejection in the collimator accounts for the observed increase in radiance within about 5˚ of the Sun. For both scattering schemes, a reduction in AOT by 0.025 at 440 nm and a corresponding increase in atmospheric absorption yield values that are much closer to measurements. The agreement is still not good perhaps because of the neglect of polarization effects in the models. However, as noted by *Lacis et al.* [1998], polarization effects cancel out when integrating radiance over angle to compute diffuse irradiance.

Figure 6

3.2. What Causes the Diffuse Discrepancy?

To understand the origin of the diffuse discrepancy, we first analyze the effect of changes in aerosol properties or other inputs to the radiative transfer models that would be required to bring the model-calculated diffuse irradiance into conformance with the observed values. This is examined in Figure 4. Consider first a low AOT case, case 27, for which the apparent AOT at 550 nm was 0.06. In Figure 4a the difference between modeled and measured diffuse irradiance, $\Delta E_{\mathrm{dif}} = E_{\mathrm{dif}}^{\mathrm{mod}} - E_{\mathrm{dif}}^{\mathrm{meas}}$, is plotted as a function of aerosol single-scattering albedo ω_0 input into the model. It is seen that a decrease in ω_0 from the observed value 0.86 to 0.46 would be required (the other input variables being held constant) to reduce ΔE_{dif} to zero from the value 18 W m^{-2} calculated for ω_0 = 0.86 (Table 1). Such a value of ω_0 is well outside the uncertainty range of its measurement and has not been encountered at the SGP ARM (midcontinental, rural) site in over 5 years of measurements (J. Ogren, NOAA, Boulder, private communication, 1998). Figure 4b shows that ΔE_{dif} cannot be reduced to zero by reducing the asymmetry parameter g from the measured value of 0.6 (holding other variables constant) for any value of g. Figure 4c likewise shows that ΔE_{dif} cannot be reduced to zero by decreasing surface reflectance ρ from the value 0.2 typical of vegetated surfaces (again holding other variables constant) for any value of ρ. For high apparent AOT, such as case 37 considered in Figure 4 with apparent AOT at 550 nm equal to 0.24, the calculated E_{dif} is much more sensitive to input parameters than for low apparent AOT, and small changes in ω_0 or g are sufficient to close the gap between models and measurements. Thus ΔE_{dif} can be made zero by reducing ω_0 from a measured value of 0.92 to 0.91 (indicated by the upward arrow in Figure 4a), a change that is within the uncertainty of the measurement (6% of 0.92 or ± 0.05). Similarly, a change in g from the measured value of 0.6 ± 0.1 to 0.55 is sufficient; such a value is again within the uncertainty range of the measurement and within the range commonly observed at SGP. Thus the discrepancy between measured and modeled E_{dif} can be sensitively examined only for

low AOT cases. For the low AOT cases, simultaneous reduction in ω_0, g and τ_{550} to 0.7, 0.4 and 0.05 (from the measured values of 0.86 ± 0.05, 0.6 ± 0.1, and 0.06 ± 0.01, respectively) reduces ΔE_{dif} to zero (paper 2). The required values of aerosol properties are still extreme. The direction of the required changes in input variables suggests that a possible origin of the discrepancy might be that a substantial fraction of particles are small (g~0) and highly absorbing ($\omega_0 \sim 0.5$).

It is suggested here and in paper 2 that radiative transfer models such as MODTRAN overestimate measured E_{dif} while correctly calculating direct irradiance E_{dir} because AOT, a key input, is overestimated. *Kato et al.* [1997] also came to the same conclusion. AOT is inferred from Sun photometer measurements of total extinction in narrow bands throughout the visible and near-IR using transmission models that compute the other two components, molecular scattering and molecular band absorption, which are subtracted from total extinction to obtain apparent AOT. There is no way to determine from extinction measurements what portion of apparent AOT is due to particles that also scatter light and what portion might be due to absorption (either by gases or by minute absorbing particles that are inefficient scatters. Historically, this residual extinction has all been ascribed to aerosols, consistent with the apparent continuous and slowly varying dependence on wavelength. If some portion of this extinction were due to absorption (over and above what can be attributed to aerosols with conventional values of ω_0), then that absorption would have to be a continuum or quasi-continuum present in two or more Sun photometer channels, because if it were not, the required absorptance in any narrow band (~10 nm wide, typical bandwidth for filters used in Sun photometers) would be huge. Such a narrowband gaseous absorption is unlikely to have remained undetected until now [*Solomon et al.*, 1998]. As noted above, all the Sun photometer channels are chosen to avoid absorption by known molecular bands, except for the Chappuis ozone band, which is accounted for during analysis of the Sun photometer data.

Column 15 in Table 1 indicates the amount of vertical optical thickness at 550 nm, $\Delta\tau_{550}$, by which the inferred AOT would have to be reduced in order to achieve closure in E_{dif}. This reduction in AOT would have to be accompanied by a corresponding increase in atmospheric absorption to maintain the closure in E_{dir}. In the model calculations used to estimate $\Delta\tau_{550}$ the increase in atmospheric absorption was simulated by reducing the extraterrestrial solar irradiance. The average value of $\Delta\tau_{550}$ for the 40 low-altitude cases is 0.022 with standard deviation 0.007; the median value is also 0.022. Assuming an Ångström exponent of -1 for the excess atmospheric absorptance, results in a corresponding hemispheric-average absorptance of 3.5%, computed as [1-exp $(-\Delta\tau_{690}/\mu)$], where μ is cos (θ), θ is the solar zenith angle equal to 60°, average for the sunlit hemisphere. This calculation assumes that the absorptance computed at 690 nm is a representative value for the entire solar spectrum. The required excess absorptance would be slightly greater (4%) for a surface reflectance of 0.2 to account for the increased absorption due to multiple reflections between the surface and the atmosphere. The uncertainty in AOT of ± 0.01, higher than the standard deviation of 0.006, determines the uncertainty in $\Delta\tau_{690}$, which translates to an uncertainty in excess absorptance of ±2%.

In cases 38-40 (BOR on September 16, 1994), measured E_{dif} was close to the Rayleigh limit (nearly aerosol-free conditions),

and AOT had to be reduced essentially to zero to achieve closure in E_{dif}. The apparent aerosol optical thickness inferred from the Sun photometer measurements exhibited a wavelength dependence represented by an Ångström exponent of 1. This apparently represents the optical thickness due to excess atmospheric continuum absorption. For all cases therefore we adopted an Ångström exponent of 1 in the radiative transfer calculations to deduce $\Delta\tau_{550}$ given in column 15 of Table 1. Note that uncertainty in AOT is ± 0.01, so that values of the Ångström exponent ascribed to the excess absorption between about 0.7 to 2 are admissible.

In an attempt to determine the cause of this excess absorption, we examined the dependence of $\Delta\tau_{550}$ on zenith angle (air mass), PW, apparent AOT, and Ångström exponent. No correlation of $\Delta\tau_{550}$ with PW or surface RH was found. Correlation with RH at some representative altitude or altitudes might be expected if the absorption were due to water dimers and trimers. This lack of correlation is consistent with the finding that the upper limit for water dimer absorption at 624 and 686 nm is about 0.001 vertical optical thickness, corresponding to an absorption of 0.8 W m^{-2}, [*Daniel et al.*, 1999] and is therefore negligible. Other chain molecules containing H_2O, O_2, N_2 are shown to also contribute negligibly to the wavelength-structured absorption in the shortwave [*Solomon et al.*, 1998]. More experimental work with water vapor at high RH is needed to fully ascertain the role of possible water continuum absorption.

Absorption by NO_2, a possible candidate absorption process arising from the presence of quasi-continuum absorption in the visible wavelengths, can be excluded as a significant contribution to the excess shortwave absorption on the basis of the absorption coefficient and representative vertical column abundance. The latter is taken as 7×10^{15} cm^{-2} (summertime maximum) based on measurements at Fairbanks, Alaska (65°N) [*Slusser et al.*, 1998]. NO_2 absorption coefficients at 380 nm (6.28×10^{-19} cm^{-2}) and 500 nm (2.1×10^{-19} cm^{-2}) [*Tomasi et al.*, 1997] yield a vertical column extinction of 0.0044 and 0.0015, respectively.

The absence of a readily identifiable gaseous source for a continuum absorption in the 300-600 nm region points to the possibility of particles as the cause (paper 2) [*Fu et al.*, 1998, 1999; *Richiazzi et al.*, 1999]. Absorption by aerosols greater than that indicated in Table 1 is apparently excluded by measurements of $\omega 0$ at the ARM site and elsewhere. However, it is necessary to revisit this conclusion in light of the fact that small aerosol particles of radius <0.05 μm may possibly contribute to this excess absorption. It is well known [e.g., *Twomey*, 1977] that for small particles, close to the Rayleigh limit, aerosol absorption is proportional to volume r^3 (where r is radius) and scattering to r^6 (square of the polarizability). Thus as the size of the particles reduces, ω_0 goes to zero. However, as noted before, ω_0 for continental aerosols measured at the ARM site and elsewhere typically has a value around 0.90. The relevant questions here are whether it is reasonable to expect low ω_0 values when the aerosol loading is low and whether sufficient concentrations of small particles could exist and persist to account for the excess absorption. It is necessary to reconcile an affirmative answer to either or both of these questions with the apparent lack of detection of aerosols having these properties with current measurement schemes. Clearly more work needs to be done to examine whether a sufficient concentration of highly absorbing small particles can and does exist with the ubiquity suggested by the present measurements.

3.3. Supporting Evidence For Diffuse Discrepancy

3.3.1. Minimum apparent AOT in Sun photometer data. Data from a worldwide network of Sun photometers belonging to the AERONET [*Holben et al.*, 1998] were examined (paper 2) to reveal a lower limit to apparent AOT at 440 nm of ~0.02. The lower limit manifested as a gap from zero in the histogram of the AOT values, revealing no occurrences below 0.02 in over 80,000 measurements at sites in North and South America and Sahelian Africa extending over a 5-year period. This period is not significantly influenced by volcanic aerosols at the locations studied. It was observed that as the wavelength decreases, the lower limit increases, consistent with the wavelength dependence of $\Delta\tau$ exhibited in the BOREAS data. In the past this minimum apparent AOT has been interpreted as background aerosol optical thickness [Forgan, 1987]. This minimum in apparent AOT could represent a nonscattering contribution to atmospheric extinction that is uniformly present at low altitude.

3.3.2. Diffuse/direct irradiance ratios. The diffuse-to-direct surface irradiance ratio has been examined in measurements by multi-filter rotating shadowband radiometer (MFRSR) [*Kato et al.*, 1997] and rotating shadowband spectrometer (RSS) [*Harrison et al.*, 1999]. An advantage of this approach is that the ratio is independent of detector calibration because the same detector is employed in both measurements; the silicon detectors employed in the MFRSR and the RSS exhibit a linear response over a wide range of intensities with no zero offset. Both of these studies found an increase in the discrepancy between modeled and measured diffuse irradiance with decreasing wavelength in the shortwave. This is consistent with the wavelength dependence (Ångström exponent $\approx$ 1) of the excess absorption inferred from BOR measurements.

3.3.3. Other supporting evidence. The problem of excess atmospheric absorption in cloudy atmospheres has been discussed since 1920 (see Stephens and Tsay [1990] for a review). In the past several years, *Cess et al.* [1995], *Ramanathan et al.* [1995], *Pilewskie and Valero* [1995], *Arking* [1995], *Imre et al.* [1996], *Li et al.* [1995], *Wild et al.* [1995], and *Charlock and Alberta* [1996] have addressed the issue of excess absorption in clear as well as cloudy atmospheres. Some of these studies interpret the problem of excess absorption as a phenomenon specific to clouds, whereas others interpret it as arising in cloud-free atmospheres but magnified in clouds because of increased multiple scattering. Several of these studies use satellite radiance to estimate top-of-the atmosphere flux. In principle, the TOA flux in conjunction with the surface flux enables calculation of atmospheric absorption, which is evaluated as the difference between net flux at TOA and net flux at the surface. However, because flux differences are measured by different sensors, absolute calibration of the satellite sensor, normally never better than ±5%, becomes important. Despite calibration issues and other problems associated with estimating broadband flux from narrowband radiance, it appears that the convergence of the results of many of these studies indicates a discrepancy between models and observations in cloud-free as well as cloudy atmospheres.

3.4. Implications of These Findings

Absorption is a fundamental process affecting energy transfer in the Earth's atmosphere. A current "textbook" estimate of shortwave atmospheric absorptance is about 20% [*Peixoto and*

Oort, 1992; *Kiehl and Trenberth*, 1997]; this value is exhibited in most radiative transfer models. This means that of the 684 W m^{-2} intercepted by the daylight side of the Earth's surface (corresponding to an average 60° solar zenith angle on the sunlit hemisphere) 136 W m^{-2} is absorbed. The excess absorption inferred from the present results (4% ± 2% absorptance) implies an additional absorption in the absence of clouds of 27 ± 14 W m^{-2}. Model (MODTRAN 3.5) simulations for a midlatitude summer cloud-free atmosphere calculate the atmospheric absorptance to be 21% without the postulated enhancement. Parameterization of absorption in other broadband models and algorithms in current global circulation models (GCMs) is close to the MODTRAN-3.5 value (R. N. Halthore et al., Intercomparison of shortwave radiative transfer codes, manuscript in preparation, 1999). This means that current GCMs may also underestimate all-sky atmospheric absorption, therefore raising concern regarding climate simulations using these models. The consequences of the omission of excess absorption indicated here on climate modeling and atmospheric circulation might be considerable.

Excess absorption over that predicted by current radiative transfer models might be expected also to affect remote sensing. First, it would affect satellite sensor calibration because atmospheric absorption must be adequately represented in models to compute at-sensor radiance. Most satellite sensors require accurate ground-look calibration after launch to supplement onboard calibration systems. Second, a satellite sensor with the wrong calibration would infer erroneous at-sensor radiance (and all that depends on it such as TOA irradiance). Third, it would affect accuracy in surface properties estimated from satellite data. The errors would be substantial. For example, an excess absorptance of 4% would lead to a decrease of ~7% in satellite sensor calibration coefficient, when the latter is expressed as radiance per count or voltage. Thus neglect of excess atmospheric absorption would lead to an overestimate of at-sensor radiance and hence to an overestimate of top-of-the atmosphere upward flux resulting in an underestimate of the computed atmospheric absorption. This subject will be elaborated in a future article.

4. Conclusions

For 40 cases at two low-altitude sites, model estimates of diffuse downward irradiance at the surface (E_{dif}) are systematically higher than those measured, in most cases by amounts that exceed combined uncertainty in model inputs and measurements. In no cases were model estimates below measured values. To some extent this conclusion is dependent on the method used to estimate daytime zero offsets in pyranometer measurements of diffuse irradiance; very large values of the offset could bring the measured values closer to the modeled values. However, such large values appear to be precluded on the basis of analysis provided here and on comparisons at two high-altitude sites where for three cases, model estimates are close to the measurements, within their mutual uncertainties. It appears that for realistic aerosol-scattering properties the model estimates can be reconciled with measurements of E_{dif} only if it is assumed that a continuum atmospheric absorption process is neglected in the radiative transfer models that compute E_{dif} and in models that extract aerosol optical thickness from Sun photometer measurements. Neglect of this excess absorption will have consequences for climate prediction and remote sensing.

Acknowledgments. We would like to acknowledge E. Mlawer (Atmospheric and Environmental Research, Inc., Cambridge, Massachusetts) for critically reviewing the manuscript and offering important suggestions, A. Berk, Spectral Sciences Inc., Boston, for help in the flux calculations using MODTRAN. MLO data were obtained from the NOAA CMDL observatory. SPO data were obtained from the BSRN data archive maintained by ETH World Radiation Monitoring Center. BOREAS data were obtained from the BOREAS database maintained at the NASA Goddard Space Flight Center. CART SGP data were obtained from the ARM program sponsored by DOE. Sun photometer data were obtained from AERONET (B. N. Holben, NASA/GSFC). 6S was made available by E. Vermote, NASA/GSFC. MODTRAN was made available by G. P. Anderson (AF Research Laboratory, Hanscom AFB, Massachusetts). Work at Brookhaven National Laboratory was supported by the Environmental Sciences Division of the U.S. Department of Energy (DOE) as part of the Atmospheric Radiation Measurement Program and was performed under the auspices of DOE under contract DE-AC02-98CH10886.

References

Anderson, G. P, et al., MODTRAN 3: Suitability as a flux-divergence code, in *Proceedings of 4th ARM Science Team Meeting*, 1994, *DOE Rep. CONF-940277*, pp. 75-80, U. S. Dep. of Energy, Washington, D. C., 1995.

Anderson, T. L., D. S. Covert, J. D. Wheeler, J. M. Harris, K. D. Perry, B. E. Trost, D. J. Jaffe, and J. A. Ogren. Aerosol backscatter fraction and single-scattering albedo: Measured values and uncertainties at a coastal station in the Pacific Northwest, *J. Geophys. Res., 104*, 26,793-26,807, 1999.

Arking, A., Absorption of solar energy in the atmosphere: Discrepancy between model and observations, *Science, 273*, 779-782, 1996.

Berk, A., L. S. Bernstein, G. P. Anderson, P. K. Acharya, D. C. Robertson, J. H. Chetwynd, and S. M. Adler-Golden, MODTRAN cloud and multiple scattering upgrades with applications to AVIRIS, *Remote Sens. Environ., 65*, 367-375, 1998.

Bernstein L. S., A. Berk, P. K. Acharya, D. C. Robertson, G. P. Anderson, J. H. Chetwynd, and L. M. Kimball, Very narrow band model calculations of atmospheric fluxes and cooling rates, *J. Atmos. Sci., 53*, 2887-2904, 1996.

Betts, A. K. and J. H. Ball, Albedo over the boreal forest. *J Geophys. Res., 102*, 28,901-28,909, 1997.

Bush, B. C., F. P. J. Valero, A. S. Simpson and L. Bignone, Characterization of thermal effects in pyranometers: A data correction algorithm for improved measurement of surface insolation, *J. Atmos. Oceanic. Technol.*, accepted, 1999.

Cess, R. D., et al., Absorption of solar radiation by clouds: Observations versus models, *Science, 267*, 496-499, 1995.

Charlock, T. P., and T. L. Alberta, The CERES/ARM/GEWEX Experiment (CAGEX) for the retrieval of radiaive fluxes with satellite data, *Bull. Am. Meteorol. Soc., 77*, 2673-2683, 1996.

Daniel, J. S., S. Solomon, R. W. Sanders, R. W. Portmann, D. C. Miller, and W. Madsen, Implications for water monomer and dimer solar absorption from observations at Boulder, Colorado, *J. Geophys. Res., 104*, 16,785-16,791, 1999.

Forgan, B.W. A New method for calibrating reference and field pyranometers, *J. Atmos. Oceanic. Technol., 13*, 638-645, 1996.

Forgan B. W. Aerosol optical depth. In *Baseline Atmospheric Program (Australia) 1985*, edited by B. W. Forgan and P. J. Fraser, 56 pp., Dep. of Sci./Bur. of Meteorol., CSIRO/Div. of Atmos. Res., Aspendale, Victoria, Australia, 1987.

Fu, Q., G. Lesins, W. Sun, and J. Higgins, Downward surface diffuse solar irradiances in clear atmospheres: Comparison between model and observations. In *Eighth ARM Science Team Meeting [1998], DOE/ER-0738*, pp. 271-276, U. S. Dep. of Energy, Washington, D. C., 1998.

Fu, Q., G. Lesins, and J. Higgins, Aerosol direct radiative forcing: A five-year climatology at the ARM SGP CART site, paper presented at the 9th Annual ARM Science Team Meeting, San Antonio, U. S. Dep. of Energy, Washington, D. C., March 22-26, 1999.

Halthore, R. N., Measurement and modeling of shortwave irradiance components in cloud-free atmospheres, in *Recent Research*

Developments in Geophysics, vol. 2, edited by S. G. Pandalai, pp. 125-139, Res. Signpost, Trivandrum, India, 1999.

Halthore, R. N., S. Nemesure, S. E. Schwartz, D. G. Imre, A. Berk, E. G. Dutton, and M. H. Bergin, Models overestimate diffuse clear-sky surface irradiance: A case for excess atmospheric absorption, *Geophys. Res. Lett., 25*, 3591-3594, 1998

Halthore, R. N., S. E. Schwartz, J. J. Michalsky, G. P. Anderson, R. A. Ferrare, B. N. Holben and H. M. Ten Brink, Comparison of model-estimated and measured direct-normal solar irradiance, *J. Geophys. Res., 102*, 29,991-30,002, 1997a.

Halthore, R. N., T. F. Eck, B. N. Holben, and B. L. Markham, Sun photometric measurements of atmospheric water vapor column abundance in the 940-nm band, *J. Geophys. Res., 102*, 4343-4352, 1997b.

Harrison, L., M. Beauharnois, J. Berndt, P. Kiedron, J. Michalsky, and Q. Min, The rotating shadowband spectroradiometer (RSS) at SGP, *Geophys. Res. Lett., 26*, 1715-1718, 1999.

Holben, B. N., et al., AERONET–A federated instrument network and data archive for aerosol characterization, *Remote Sens. Environ., 66*, 1-16, 1998.

Imre, D. G., E. H. Abramson, and P. H. Daum, Quantifying cloud-induced shortwave absorption: an examination of uncertainties and of recent arguments for large excess absorption, *J. Appl. Meteorol., 35*, 1991-2010, 1996.

Kato, S., T. P. Ackerman, E. E. Clothiaux, J. H. Mather, G. G. Mace, M. L. Wesely, F. Murcray, and J. Michalsky, Uncertainties in modeled and measured clear-sky surface shortwave irradiances, *J. Geophys. Res., 102*, 25,881-25,898, 1997.

Kiehl, J. T., and K. E. Trenberth, Earth's annual global mean energy budget, *Bull. Am. Meteorol. Soc., 78*, 197-208, 1997.

Lacis, A. A., J. Chowdhary, B. Cairns, and M. I. Mishchenko, Modeling errors in diffuse-sky radiation, *Geophys. Res. Lett., 25*, 135-138, 1998.

Li, Z., H. W. Barker, and L. Moreau, The variable effect of clouds on atmospheric absorption of solar radiation, *Nature*, 376, 486-490, 1995.

Marshall, S. F., D. S. Covert, and R. J. Charlson, Relationship between asymmetry parameter and hemispheric backscatter ratio: Implications for climate forcing by aerosols, *Appl. Opt*., *34*, 6306-6311, 1995.

Neuendorffer, A., Ozone monitoring with TIROS-N operational vertical sounders, *J. Geophys. Res., 101*, 18,807-18,828, 1996.

Ohmura, A. and K. Schroff, Physical characteristics of the davos-type pyrradiometer for short- and long-wave radiation, *Arch. Meteorol. Geophys. Bioclim., Ser. B, 33*, 57-76, 1983.

Peixoto J. P. and A. H. Oort, *Physics of Climate*, Am. Inst. of Phys., New York, 1992.

Pilewskie, P., and F. P. J. Valero, Direct observations of excess solar absorption by clouds, *Science*, 257, 1626-1629, 1995.

Ramanathan, V., B. Subasilar, G. J. Zhang, W. Conant, R. D. Cess, J. T. Kiehl, H. Grassl, and L. Shi, Warm pool heat budget and shortwave cloud forcing: A missing physics?, *Science, 267*, 499-503, 1995.

Ricchiazzi, P., C. Gautier, and T. P. Tooman, Spectral and angular characteristics of diffuse solar radiation due to aerosol, paper presented at the Ninth Atmospheric Radiation Measurement (ARM) Science Team Meeting, San Antonio, U. S. Dep. of Energy, Washington, D. C., 1999.

Rothman, L.S., et al., The HITRAN molecular spectrscopic database and HAWKS (HITRAN atmsopheric workstation): 1996 edition, *J. Quant. Spectrosc. Radiat. Transfer, 60*, 665-710, 1998.

Slusser J., X. Liu , K. Stamnes, G. Shaw, R. Smith, R. Storvold, F. Murcray, A. Lee, and P. Good, High-latitude stratospheric NO_2 and HNO_3 over Fairbanks (65°N) 1992-1994. *J. Geophys. Res., 103*, 1549-1554, 1998.

Solomon, S., R. W. Portmann, R. W. Sanders, and J. S. Daniel, Absorption of solar radiation by water vapor, oxygen, and related collision pairs in the Earth's atmosphere, *J. Geophys. Res., 103*, 3847-3858, 1998.

Stamnes K., S.-C. Tsay, W. J. Wiscombe, and K. Jayaweera, Numerically stable algorithm for discrete-ordinate-method radiative transfer in multiple scattering and emitting layered media, *Appl. Opt., 27*, 2502-2509, 1988.

Stephens, G. L. and S. -C. Tsay, On the cloud absorption anomaly. *Q. J. R. Meteorol. Soc., 116*, 671-704, 1990.

Tomasi C., V. Vitale, and L. Tarozzi, Sun-photometric measurements of atmospheric turbidity variations caused by the pinatubo aerosol cloud in the Himalayan region, *Nuovo Cimento Soc. Ital. Fis., 20*, 61-88, 1997.

Trishchenko, A. and Z. Li, A synergetic study of solar fluxes and aerosol properties under clear-sky conditions, in *Eighth ARM Science Team Meeting [1998], DOE/ER-0738*, pp. 761-765, U. S. Dep. of Energy, Washington, D. C., 1998.

Twomey S., *Atmospheric Aerosols*, Elsevier, New York, 1977.

Vermote E. F., D. Tanre, J. L. Deuze, M. Herman, and J. J. Morcrette, Second simulation of the satellite signal in the solar spectrum (6S), *IEEE Trans. Geosci. Remote Sens.*, *35*, 3, 1997.

Walter-Shea, E. A., B. L. Blad, C. J. Hays, M. A. Mesarch, D. W. Deering, and E. M. Middleton, Biophysical properties affecting vegetative canopy reflectance and absorbed photosynthetically active radiation at the FIFE site, *J Geophys. Res.*, *97*, 18,925-18,934, 1992.

Wardle, D. I., and D. V. Barton, Zero offsets in pyranometer signals related to long-wave radiation, temperature change and ventilation and some implications regarding measurements uncertainty, *Rep. ARPD 129X52*, 36 pp., Atmos. Environ. Serv., Downsview, Canada, 1988. (Available from Environ. Can., Downsview, Ontario, Canada.)

Wardle, D. I., L. Dahlgren, K. Dehne, L.Leidquist, L. J. B. McArthur, Y. Miyake, O. Motschka, C. A. Velds, and C. V. Wells, Improved measurement of solar irradiance by means of detailed pyranometer characterization, *Rep. IEA-SHCP-9C-2*, Int. Energy Agency, Paris, France, 1996. (Available from Environ. Can., Downsview, Ontario, Canada.)

Warren, S. G., and Wiscombe, W. J., A Model for the spectral albedo of snow, II, snow containing atmospheric aerosols, *J. Atmos. Sci.*, *37*, 2734-2743, 1981.

Wild, M., A. Ohmura, H. Gilgen, and E. Roeckner, Validation of GCM simulated radiative fluxes using surface observations, *J. Clim.*, *8*, 1309-1324, 1995.

Wiscombe, W. J., An absorbing mystery, *Nature*, *376*, 466-467, 1995.

R. N. Halthore and S. E. Schwartz, Atmospheric Sciences Division, Environmental Sciences Department, Brookhaven National Laboratory, Building 815E, Upton, NY 11973-5000. (halthore@bnl.gov)

(Received November 30, 1999; revised March 31, 2000;
accepted April 4, 2000.)

Copyright 2000 by the American Geophysical Union.

Paper number 2000JD900224.
0148-0227/00/2000JD900224$09.00

Table 1. Summary of Results

1	2	3	4	5	6	7	8	9	10	11	12	13	14	15
Case	Date	Time, UT	Solar zenith Angle, deg	Apparent AOT at 550 nm	Ångström Exponent	ω_0[a]	g[a]	PW[b], cm	Zero Offset[c] W m^{-2}	E_{dif}, (Measured) W m^{-2}	E_{dif}, (2 stream)[d] W m^{-2}	E_{dif}, (8 stream)[d] W m^{-2}	ΔE_{dif} W m^{-2}	ΔAOT
1	April 13, 1996	1434:05	59.69	0.12	0.74	0.94	0.58	(0.98)	6	96	104	105	9	0.015
2	April 13, 1996	1445:27	57.46	0.12	0.72	0.94	0.60	(0.99)	6	97	108	108	11	0.018
3	April 15, 1996	1459:55	54.12	0.06	1.6	0.94	0.60	0.78	7	64	80	80	16	0.024
4	April 18, 1996	1412:36	62.66	0.10	0.58	0.94	0.58	1.09	9	79	90	91	12	0.017
5	April 18, 1996	1427:30	59.70	0.10	0.58	0.94	0.55	1.09	9	83	93	95	12	0.020
6	April 18, 1996	1434:04	58.40	0.09	0.6	0.94	0.60	1.09	9	84	95	96	12	0.019
7	April 18, 1996	1444:13	56.40	0.10	0.6	0.94	0.57	1.09	9	86	100	101	15	0.022
8	April 18, 1996	1714:17	30.54	0.08	0.7	0.94	0.55	0.66	9	90	110	114	24	0.027
9	April 18, 1996	1729:16	28.82	0.08	0.65	0.94	0.55	0.66	9	93	112	116	23	0.024
10	April 18, 1996	1744:15	27.41	0.08	0.7	0.94	0.66	0.66	9	93	113	117	24	0.028
11	April 19, 1996	1714:04	30.25	0.08	0.71	0.94	0.60	1.11	6	87	112	116	29	0.035
12	April 19, 1996	1729:03	28.51	0.07	0.85	0.94	0.60	1.11	6	85	104	108	23	0.028
13	April 19, 1996	1744:03	27.08	0.08	0.74	0.94	0.61	1.11	6	89	114	118	29	0.034
14	April 19, 1996	2325:24	70.48	0.12	0.5	0.94	0.74	0.92	7	70	87	88	18	0.031
15	April 19, 1996	2335:06	72.42	0.12	0.5	0.94	0.71	0.92	7	69	83	85	16	0.031
16	April 19, 1996	2337:12	72.84	0.13	0.48	0.94	0.67	0.92	7	69	84	86	17	0.031
17	April 23, 1996	1328:54	70.23	0.13	1.0	0.94	0.72	0.91	6	80	88	88	8	0.016
18	April 23, 1996	1338:29	68.31	0.14	1.0	0.94	0.74	0.91	6	85	94	94	9	0.017
19	April 23, 1996	1344:37	67.08	0.14	1.0	0.94	0.76	0.91	6	88	97	97	9	0.018
20	April 23, 1996	1354:34	65.08	0.14	1.0	0.94	0.75	0.91	6	92	102	102	11	0.020
21	April 23, 1996	1406:38	62.67	0.13	1.0	0.94	0.75	0.91	7	96	105	105	9	0.016
22	April 23, 1996	1421:30	59.70	0.13	1.0	0.94	0.76	0.91	7	98	110	110	12	0.020
23	April 23, 1996	1428:14	58.36	0.13	1.0	0.94	0.73	0.91	7	100	111	111	11	0.019
24	Sept. 18, 1997	1422:53	65.35	0.12	1.35	(0.92)	(0.70)	4.23	9	80	88	91	11	0.022
25	Sept. 18, 1997	2300:48	72.50	0.12	1.1	(0.92)	(0.60)	3.79	15	68	71	76	8	0.017
26	Sept. 27, 1997	1420:59	67.20	0.07	1.3	(0.86)	(0.60)	2.58	7	54	63	66	12	0.025
27	Sept. 27, 1997	1721:39	40.29	0.06	1.5	(0.86)	(0.60)	2.54	7	69	84	87	18	0.029
28	Sept. 29, 1997	1433:49	65.41	0.03	1.01	(0.76)	(0.50)	1.44	7	51	53	55	4	0.010
29	Sept. 29, 1997	2022:53	48.59	0.04	1.05	(0.83)	(0.50)	1.45	7	59	70	74	15	0.024
30	Sept. 29, 1997	2324:38	80.54	0.04	1.04	(0.79)	(0.50)	1.55	7	29	33	37	8	0.022
31	Sept. 30, 1997	1722:34	41.77	0.07	1.42	(0.85)	(0.50)	1.97	7	78	88	91	13	0.022
32	Sept. 30, 1997	2052:48	53.29	0.06	1.16	(0.84)	(0.50)	1.96	8	66	77	79	13	0.026
33	Sept. 30, 1997	2327:00	81.41	0.08	1.08	(0.83)	(0.50)	2.09	8	33	34	40	7	0.024
34	Oct. 01, 1997	1749:55	40.57	0.13	1.6	(0.88)	(0.50)	2.94	6	107	115	117	10	0.017
35	Oct. 01, 1997	2019:40	48.97	0.14	1.6	(0.88)	(0.50)	2.95	6	105	111	113	8	0.013
36	Oct. 01, 1997	2324:00	81.02	0.14	1.7	(0.83)	(0.50)	3.08	6	40	37	44	4	0.012
37	Oct. 04, 1997	2034:00	51.39	0.24	1.6	(0.92)	(0.60)	3.26	11	141	143	143	2	0.004
38[e]	Sept. 16, 1994	1531:00	65.44	0.03	1.15	0.94	0.60	1.55	0	42	55	54	12	0.023
39[e]	Sept. 16, 1994	1631:00	59.53	0.03	1.11	0.94	0.60	1.55	0	44	60	59	15	0.025
40[e]	Sept. 16, 1994	1631:00	58.03	0.03	1.16	0.94	0.60	1.55	0	44	61	62	18	0.027
41[f]	Dec. 24, 1997	1736:30	81.67	0.01	1.1	0.94	0.60	0.11	8	26	24	24	-2	0.000
42[f]	Dec. 24, 1997	1921:31	61.47	0.01	1.1	0.94	0.60	0.11	10	39	38	38	-1	0.000
43[g]	Nov. 16, 1995	1300:00	71.47	0.00	–	–		0.12	0	48	46	46	-2	0.000

[a]Measured values are in parentheses, rest, assumed.
[b]from Sun photometers (in parentheses) and radiosondes.
[c]for some cases with pre-applied offsets, values are zero (see text).
[d]MODTRAN 3.5.
[e]BOREAS.
[f]MLO.
[g]SPO; all others, SGP.

Table 2. Summary of Sensitivity Analyses

1	2	3	4	5	6	7	8	
							$\delta(\Delta E_{dif})$[a], W m^{-2}	
Case	AOT (550 nm)	$\partial E_{dif}/\partial\rho$ W m^{-2}, ($\delta\rho$=0.1)[b]	$\partial E_{dif}/\partial\tau$ W m^{-2}, ($\delta\tau$=0.01)[b]	$\partial E_{dif}/\partial\omega_0$ W m^{-2}, ($\delta\omega_0$=6%)[b]	$\partial E_{dif}/\partial g$ W m^{-2}, (δg=0.1)[b]	δE_{dif} W m^{-2}	75%	95%
27	0.06	30	500	47	20	6.8	8.4	10.5
34	0.13	30	500	105	40	9.5	10.7	12.4
37	0.25	25	500	186	60	13.9	14.8	16.0

[a]ΔE_{dif} is the difference between modeled and measured E_{dif}.
[b]uncertainty in these quantities; δ=uncertainty.

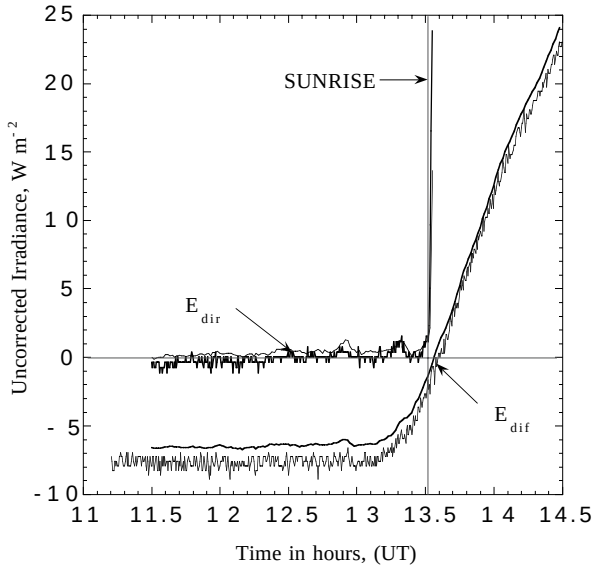

Figure 1. Pyrheliometer-measured E_{dir} and uncorrected pyranometer-measured E_{dif} obtained on a cloud-free day (December 10, 1996) at Southern Great Plains (SGP) by two groups of instruments, BSRN (smooth lines, 1-min average of 1-s data) and SIRS (noisier lines, instantaneous values every 20 s), are plotted versus time. At sunrise, indicated by a steep rise in E_{dir}, uncorrected E_{dif} is negative when diffuse sky irradiance is clearly positive. Local clock time is (UT - 6) hours.

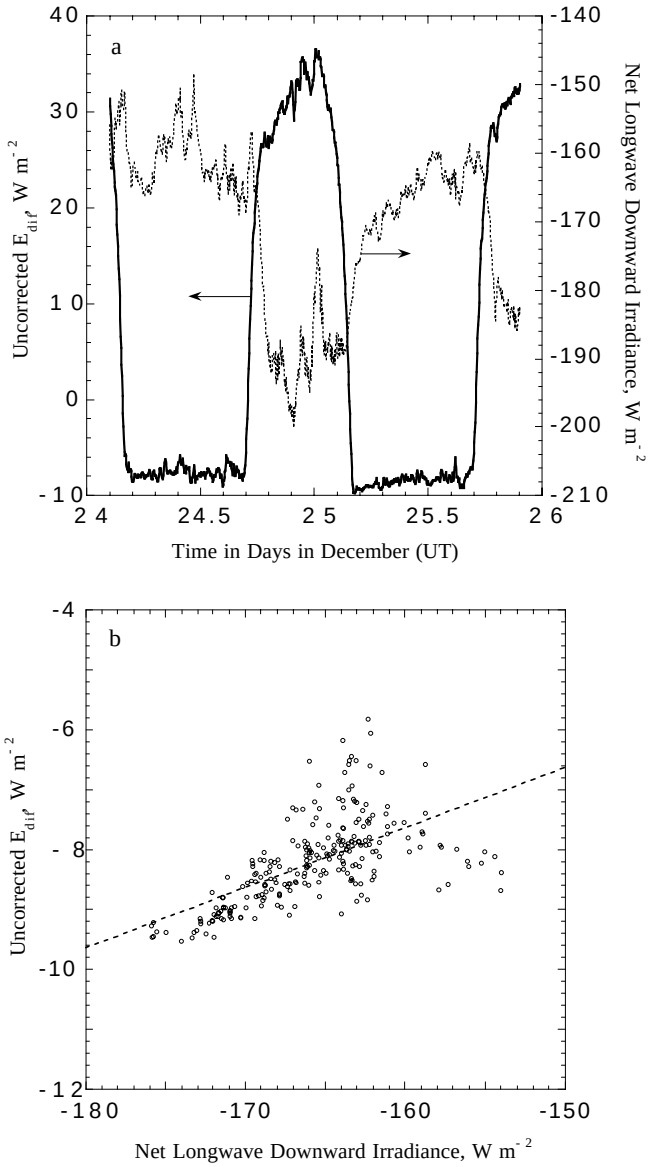

Figure 2. (a) Diffuse pyranometer signal, i.e., uncorrected E_{dif}, and net longwave surface irradiance as measured by an uplooking pyrgeometer are plotted versus time of day (fractional days, UTC) in December 1997 at Mauna Loa in Hawaii (MLO); local clock time is UT, 10 hours. (b) Nighttime (24.2-24.671 and 25.177-25.615 in days UT) values of uncorrected E_{dif} is plotted against longwave flux (r^2=0.4). Data represent 1-min averages of 1-s data.

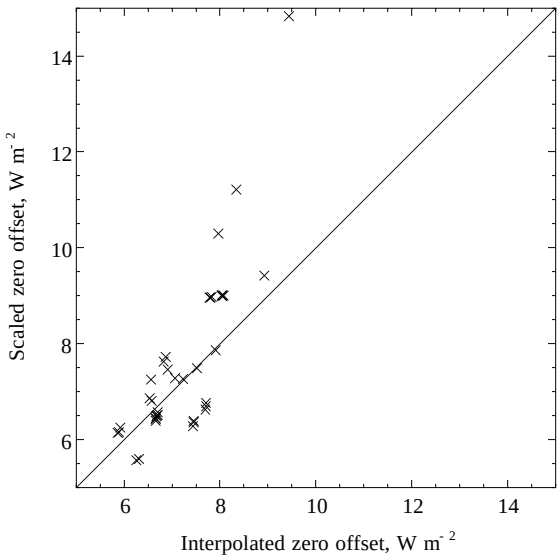

Figure 3. Zero offset obtained by scaling to the pyrgeometer signal is plotted against zero offset obtained by interpolation or extrapolation of nighttime offsets in one or both of previous and successive nights. All cases in Table 1 at SGP and MLO are represented. One-to-one line is indicated by the solid line.

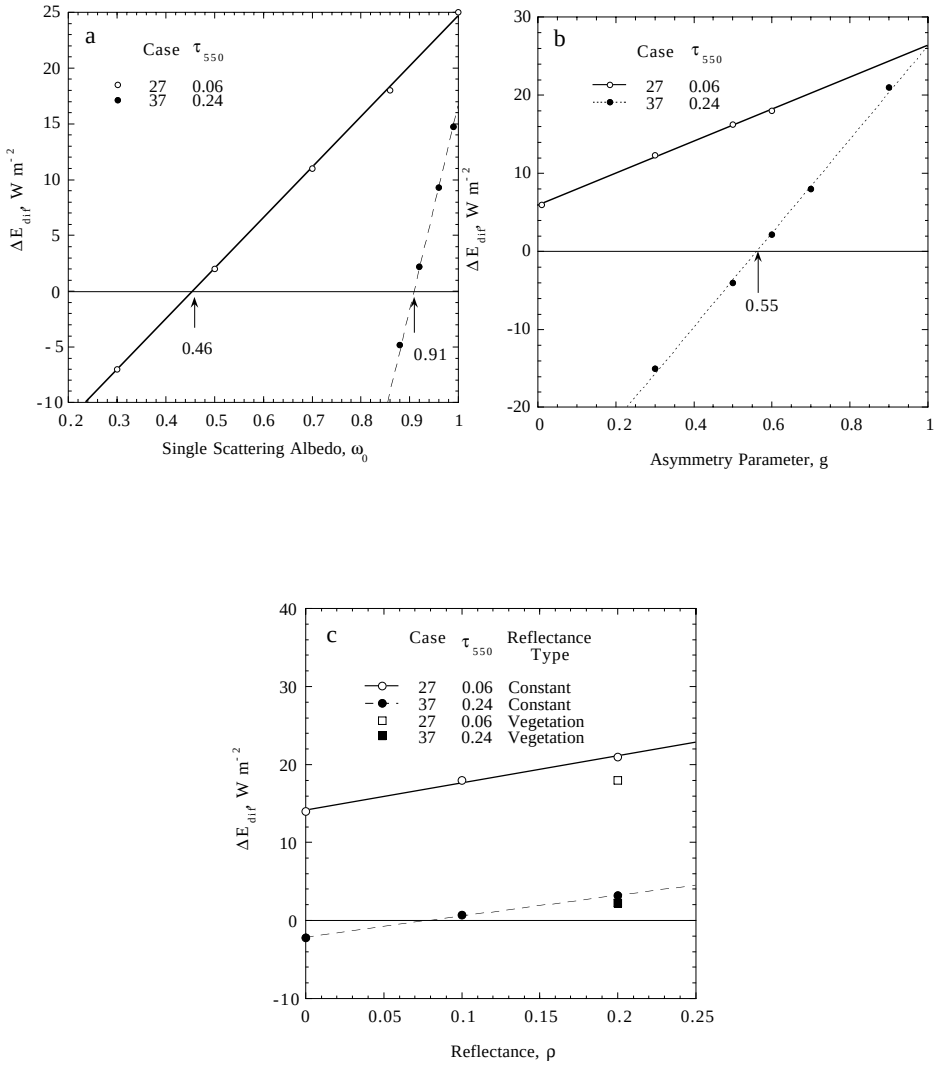

Figure 4. Sensitivity of modeled diffuse irradiance E_{dir} to changes in (a) single-scattering albedo ω_0, (b) asymmetry parameter g, and (c) surface reflectance ρ is shown. In each plot the difference between modeled and measured E_{dif} is given for a low aerosol optical thickness (AOT) case (τ_{550} = 0.06, September 27, 1997; case 27, open circles) and a high AOT case (τ_{550} = 0.24, October 4, 1997; case 37, solid circles). Measured E_{dif} is 68 W m^{-2} for the low AOT case 27, and 141 W m^{-2} for the high AOT case 37. (b) For the low AOT case 27, the modeled E_{dif} cannot be reduced to the measured value by any physically plausible value of g. (c) Circles represent cases for which the surface reflectance is assumed constant with wavelength, and squares represent cases using a surface reflectance for a vegetated surface (integrated reflectance is equal to 0.2). The open and solid symbols represent low and high AOT cases, respectively.

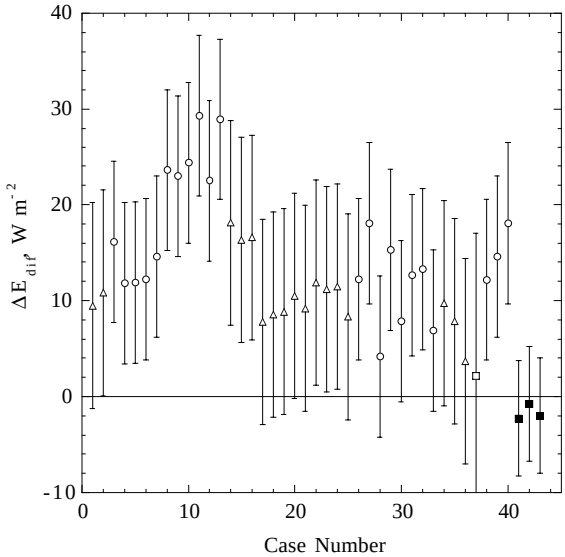

Figure 5. Difference between modeled (eight streams) and measured diffuse irradiance, $\Delta E_{\mathrm{dif}} = E_{\mathrm{dif}}^{\mathrm{mod}} - E_{\mathrm{dif}}^{\mathrm{meas}}$ is shown for each case in Table 1, with uncertainties at the 75% confidence level (Table 2). Uncertainties are dependent on AOT: low AOT ($\tau_{550} \leq 0.1$, open circles), intermediate AOT ($0.1 < \tau_{550} \leq 0.2$, open triangles), and high AOT ($\tau_{550} > 0.2$, open square). High-altitude cases (solid squares) exhibit lower uncertainties because of very low AOT (<0.01).

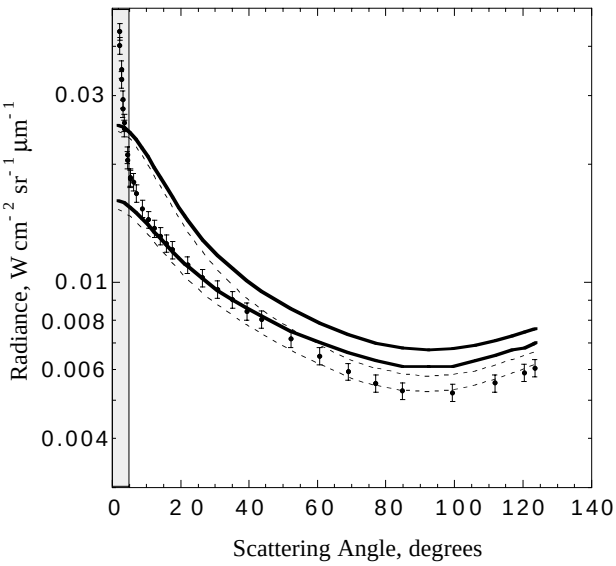

Figure 6. Sky radiance is shown along the almucantar (i.e., at constant viewing zenith angle equal to solar zenith angle of ~62° and variable azimuth angle). Radiance measured at 440 nm by a calibrated radiometer (circles with ±5% uncertainty) at 1400 UTC (local clock time is UTC, 6 hours) on September 16, 1994, at BOR, is plotted against scattering angle and compared with model calculations by MODTRAN-3.5 eight stream (solid line) and two stream (dotted line). Top curves for each calculation are for uncorrected AOT as inferred from the same instrument in the Sun photometer mode of operation. Bottom curves are obtained by reducing AOT at 440 nm by 0.025. Values for scattering angle near zero are shaded to denote contamination by direct solar radiance.